CONF-970201--7 SAND 96-0951C SAND--96-0951C

Modeling Non-Isothermal Intermetallic Layer Growth in the 63Sn-37Pb/Cu System*

P. T. Vianco, P. L. Hopkins, K. L. Erickson, D. R. Frear, and R. Davidson

Sandia National Laboratories
Albuquerque, New Mexico 87185

RECEIVED
NOV 05 1996
OSTI

Abstract

The reliability of mechanical and electronic systems can be acutely dependent on the integrity of the soldered joints used in the assembly. During product manufacture, intermetallic layers form in reaction zones between the dissimilar materials of solder joints. Thermal cycling during service can cause further growth of the intermetallic layers, which may jeopardize the mechanical integrity of the joints. Models describing such service related changes are essential in predicting the long-term mechanical reliability of these interconnects. Previously (1-3), a model describing the diffusion-controlled growth of multiple intermetallic layers and the displacement of the interfaces between layers was developed and implemented in a one-dimensional computer code based on the method-of-lines. The computer code was applied to the analysis of intermetallic layer growth in isothermal solder aging experiments performed with 100 Sn/Cu and 63Sn-37Pb/Cu solder-substrate systems. The analyses indicated that intermetallic layer growth was consistent with a bulk diffusion mechanism involving Cu and (or) Sn. In this work, nonisothermal solder-aging experiments were done with the 63Sn-37Pb/Cu system using two temperature histories: (1) a low frequency history consisting of 4 cycles per day between 223 K and 443 K and (2) a high frequency history consisting of 72 cycles per day between 223 K and 443 K. Isothermal experiments at 443 K also were done. Thicknesses of both the Cu_3Sn and Cu_6Sn_5 intermetallic layers were determined as a function of time for each temperature history. An updated version of the previously developed model and code were used to predict the intermetallic layer growth for both nonisothermal temperature histories. Arrhenius expressions for diffusion coefficients in both the Cu_3Sn and Cu_6Sn_5 layers were determined using experimental data from the previous isothermal studies. Agreement between predicted and experimental results was generally good. In some cases, predicted layer growth was less than experimentally observed, but within experimental error. This paper describes the nonisothermal experiments and a comparison of the predicted and observed layer growth as a function of time.

Introduction

The reliability of mechanical and electronic systems can be acutely dependent on the integrity of the soldered joints used in the assembly. During product manufacture, intermetallic compound (IMC) layers form in reaction zones between the dissimilar materials of solder joints. Thermal cycling during service can cause further growth of the intermetallic layers, which may jeopardize the mechanical integrity of the joints as well as their capacity for subsequent rework or repair. Models describing service caused changes to solder joint microstructure, such as IMC growth are essential in understanding and predicting the long-term mechanical reliability and serviceability of these interconnects.

In previously published work (1-3), a model describing the diffusion-controlled growth of multiple intermetallic layers and the displacement of the interfaces between layers was developed and implemented in a one-dimensional computer code based on the method-of-lines. The model could accommodate cases involving: (1) finite initial layer thicknesses, (2) rate-limiting interfacial reactions, (3) multiple and variable diffusion coefficients, and (4) finite material boundaries. Additionally, the effects of nucleation could be modeled empirically. A transformation of the spatial coordinate circumvented the need to remesh the growing and (or) shrinking layers. Results from the one-dimensional code were verified by comparing the numerical results with analytical solutions for simple systems involving two, three, and five layers.The computer code was then applied to the analysis of intermetallic layer growth from isothermal solder aging experiments done with 100 Sn/Cu and 63Sn-37Pb/Cu solder-substrate systems. The 63Sn-37Pb/Cu experiments were done at temperatures of 343, 373, 408 and 443 K. The 100Sn/Cu experiments were done at the same temperatures as well as at 478 K. The analyses indicated that intermetallic layer growth was consistent with a bulk diffusion mechanism involving Cu and (or) Sn and variable diffusion coefficients that reflect some enhanced diffusion during early layer growth.

In this work, nonisothermal solder-aging experiments were done with the 63Sn-37Pb/Cu system using two temperature histories: (1) a low frequency history consisting of 4 cycles per day between 223 K and 443 K and (2) a high frequency history consisting of 72 cycles per day between 223 K and 443 K. Isothermal experiments at 443 K also were done. Thicknesses of both the Cu_3Sn and Cu_6Sn_5 intermetallic layers were determined as a function of time for both temperature histories. An updated ver-

*This work was performed at Sandia National Laboratories and supported by the U. S. Department of Energy under contract DE-AC04-94AL85000.

DISTRIBUTION OF THIS DOCUMENT IS UNLIMITED

MASTER

DISCLAIMER

This report was prepared as an account of work sponsored by an agency of the United States Government. Neither the United States Government nor any agency thereof, nor any of their employees, make any warranty, express or implied, or assumes any legal liability or responsibility for the accuracy, completeness, or usefulness of any information, apparatus, product, or process disclosed, or represents that its use would not infringe privately owned rights. Reference herein to any specific commercial product, process, or service by trade name, trademark, manufacturer, or otherwise does not necessarily constitute or imply its endorsement, recommendation, or favoring by the United States Government or any agency thereof. The views and opinions of authors expressed herein do not necessarily state or reflect those of the United States Government or any agency thereof.

sion of the previously developed model and code were used to predict the nonisothermal intermetallic layer growth for both temperature histories. Arrhenius expressions for diffusion coefficients in both the Cu_3Sn and Cu_6Sn_5 layers were determined using experimental data from the previous isothermal studies. Agreement between predicted and experimental results was generally good. In some cases, predicted layer growth was less than experimentally observed, but within experimental error. This paper summarizes the current isothermal and nonisothermal experimental procedures and results and provides a brief description of the updated layer-growth model and its numerical implementation. Predicted IMC layer growth as a function of time for all three temperature histories are compared with the corresponding experimental results, and apparent differences between predicted and observed results are discussed.

Experiment

Procedure

The experimental procedures used to obtain data for intermetallic layer growth between 63Sn-37Pb solder and Cu substrates are described below. Data for layer growth were obtained from both the isothermal and non-isothermal aging experiments.

Samples for the thermal aging experiments were obtained from pairs of Cu substrates separated by specified gaps that were filled with solder. The substrates were oxygen-free, high conductivity (OFHC) copper plates, which were rectangular in shape, 25.4 by 50.8 mm, and 0.51 mm thick. Copper spacers were welded onto one substrate of each pair. The thicknesses of the spacers were varied to provide the following gap widths between the substrates: 76 μm, 128 μm, 254 μm, and 381 μm. Each pair of plates, which were still separate, was then etched for 30 s in a 1:1 by volume solution of HCl and water; rinsed, and dried in flowing nitrogen. The surfaces that formed the walls of the gap when the plates were joined were coated with a rosin-based, mildly activated (RMA) flux. The two plates were then spot welded together so that the spacers formed a controlled gap having one of the above mentioned thicknesses. Each sample was immersed to a depth of 1 mm in a bath of molten 63Sn-37Pb (wt.%) solder that was at 533 K. Each specimen was kept in the solder for a time period of 60 s. The specimen was then removed from the solder, allowed to cool, and any remaining flux residues removed using organic solvents. The specimens were sectioned into samples that were 25.4 by 6 mm.

All thermal aging experiments were done in air furnaces. The temperature histories used in the experiments are referred to as follows: (1) *isothermal*, (2) *nonisothermal, slow cycle rate*, and (3) *nonisothermal, fast cycle rate*, and represented maximum IMC growth conditions for the comparative assessment. For all three temperature histories, the aging experiments were done for time periods of 10, 40, and 100 days.The isothermal experiments were done at a temperature of 443 K. The nonisothermal, slow cycle experiments involved 4 cycles per day. In each cycle, the temperature increased linearly from 223 to 443 K during a time period of 1 hour, remained at 443 K during the next two hours, decreased linearly to 223 K during the fourth hour, and remained at 223 K during the next two hours. The nonisothermal, fast cycle experiments involved 72 cycles per day. In each cycle the temperature increased linearly from 223 to 443 K during the first five-minute period, remained at 443 K for a five minute period, decreased linearly to 223 K during the next five-minute period, and then remained at 223 K during the next five-minute period. One sample from each of the four gap widths was exposed to one of the isothermal and nonisothermal temperature histories. In the nonisothermal experiments, a thermocouple was attached to one of the samples, so that the temperature history was accurately controlled and known.

At the specified time intervals mentioned above, the samples were removed from the test apparatus. Each sample was cross sectioned along the long dimension. One section from each sample was mounted and metallographically polished. Measurements of IMC layer thicknesses were done as follows: three positions were selected along the gap length; one position was located at the center of the sample, and the other two positions were located on either side at a distance of 9.53 mm from the center. At each location, ten thickness measurements were taken of the IMC layer on each side of the gap from 100x micrographs. The measurement error was ± 0.3 μm. The two sets of ten measurements per location were combined to determine an average IMC layer thickness at each location. The same IMC layer thickness analysis was done for each of the sub-layers, Cu_3Sn and Cu_6Sn_5, that comprised the total IMC layer. The data per location and gap thickness were represented by the mean of the twenty thickness values and ± one standard deviation of those values.

Results

Figure 1 shows the IMC layer which developed during an isothermal aging period of 10 days at a temperature of 443 K. The IMC layer is composed of two sublayers, the Cu_3Sn sublayer (darker gray) next to the copper substrate, and the Cu_6Sn_5 (lighter gray) next to the 63Sn-37Pb solder field. Isothermal aging for a period of 100 days at a temperature of 443 K produced a considerably thicker IMC layer, which is shown in Figure 2. In addition, a Pb-rich zone developed ahead of the IMC layer, at the interface between the Cu_6Sn_5 sublayers and the solder field.

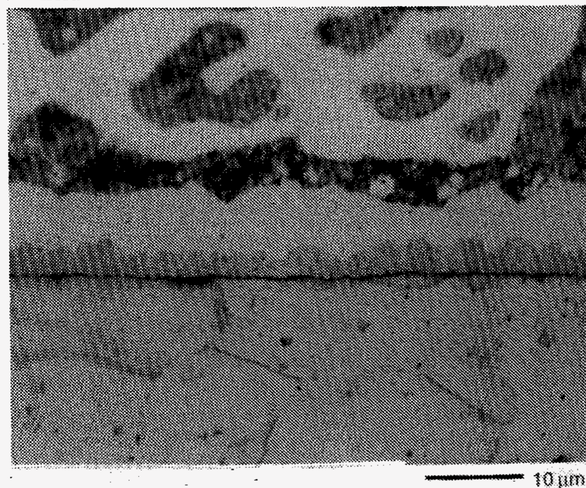

Figure 1. Micrograph showing IMC layer after an isothermal aging period of 10 days at a temperature of 443 K.

The IMC layer thickness data obtained from the *fast-cycle*, non-isothermal aging experiments are shown in Tables I - III. Data from the left position off the centerline are shown in Table I; thickness data from the centerline position in Table II, and data from the right position off the centerline in Table III. The results are given for each of the four gap dimensions at aging time periods of 10 and 40 days and for the smallest and largest gap dimensions at 100 days. The data in Tables I - III illustrate four important points that are pertinent to layer growth kinetics in both *fast-* and *slow-cycle*, non-isothermal experiments, as well as the isothermal experiments.

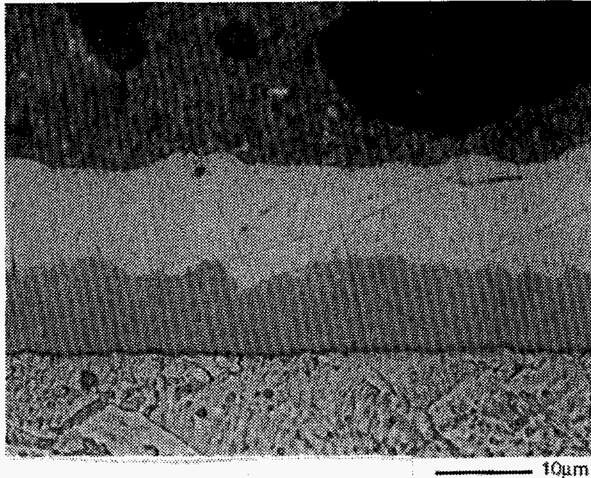

Figure 2. Micrograph showing IMC layer after an isothermal aging period of 100 days at a temperature of 443 K.

First, the data in Tables I - III show that within experimental error, both of the sublayers, Cu_3Sn and Cu_6Sn_5, and the total layer thicknesses were not functions of position along the gap of each respective sample. In view of the thermal expansion mismatch between Cu and 63Sn-37Pb solder, 17.0 ppm/K and 25.0 ppm/K, respectively, (4) this result indicates that for each of the test conditions, any residual stress field that formed in the joint region did not impact the extent of growth of either of the sub-layers, or growth of the IMC layer as a whole.

Second, the data in Tables I - III show that IMC layer growth was not sensitive to the tested range of gap sizes. A trend appeared to be present in the 100-day (6151 cycles) data, in which the Cu_3Sn sub-layer that formed in the IMC layers with the 381 µm gap was apparently larger than the Cu_3Sn sublayer formed with the 76 µm gap. Conversely, the Cu_6Sn_5 sublayer thickness was smaller with the 381 µm gap, so that the total layer thickness remained about equal between the two gap sizes. However, the apparent differences in the sub-layer thicknesses, although reproduced at each of the positions along the gap, were within the experimental error of the measurements, and therefore, could not be considered statistically significant.

Third, based on the data scatter (standard deviation), neither the position along the gap nor the gap thickness had an impact on the *variability* of the IMC layer thickness data.

Finally, because the total thickness of the IMC layer and the thicknesses of each of the sub-layers did not exhibit significant trends as a function of position within each sample, nor as a function of the gap thickness, these data typify the thickness variability that can be expected from the measurement technique as well as the inherent variability in layer growth in this material system.

The IMC layer thickness data obtained from the *slow-cycle*, non-isothermal aging experiments are shown in Table IV. The values given were obtained by combining the data from each of the left, center, and right positions along the gap of the respective specimens. In general, the IMC layer and sub-layer thicknesses obtained in the *slow-cycle* experiments were not significantly different from those obtained in the *fast cycle* experiments. Since each test cycle, of both test cycle regimes, caused the respective samples to spend about one-half of the test time above the baseline temperature of 298 K and one-half below 298 K, and since the test duration rather than the number of cycles was controlled, similar IMC layer thicknesses would be anticipated in the absence of other extraneous factors. This trend was indeed observed in the experimental data. However, the scatter in the data from the *slow-cycle* experiments tended to be greater than that from the *fast-cycle* experiments.

The combined data from the *isothermal* experiments at 443 K that were done for the same time periods are shown in Table V. In the *isothermal* experiments, the specimens were exposed to the elevated temperature for the entire duration of the aging period. Therefore, the IMC layer thicknesses would be expected to be greater when compared with data from non-isothermally tested specimens. This trend was confirmed. Also, when compared as a percent variation about the mean value, the scatter in the data from the isothermal aging experiments was approximately at a level between data scatters of the two nonisothermal temperature histories.

Table I: IMC Layer Thickness from Non-Isothermal Aging, Fast Cycle Rate, Left of Center.

Time (Days)	Gap (mm)	Ave. Layer Thickness (Std. Dev.) (µm)		
		Cu_3Sn	Cu_6Sn_5	Total
10	76	1.79 (0.37)	3.36 (0.95)	5.15 (0.66)
	128	1.76 (0.33)	3.47 (0.69)	5.23 (0.46)
	254	1.72 (0.24)	3.53 (.57)	5.24 (0.41)
	381	1.71 (0.32)	4.76 (0.91)	6.46 (0.69)
40	76	3.02 (0.62)	5.53 (1.34)	8.55 (1.00)
	128	2.93 (0.60)	5.87 (1.16)	8.80 (0.72)
	254	2.71 (0.58)	5.01 (1.25)	7.72 (0.88)
	381	2.84 (0.58)	6.02 (0.91)	8.87 (0.65)
100	76	3.61 (0.64)	8.18 (1.94)	11.79 (1.74)
	128	—	—	—
	254	—	—	—
	381	4.44 (0.71)	6.65 (1.38)	11.10 (0.97)

Table II: IMC Layer Thickness from Non-Isothermal Aging, Fast Cycle Rate, Center.

Time (Days)	Gap (mm)	Ave. Layer Thickness (Std. Dev.) (μm)		
		Cu_3Sn	Cu_6Sn_5	Total
10	76	1.68 (0.41)	3.55 (0.82)	5.22 (0.51)
	128	1.86 (0.40)	3.40 (0.93)	5.26 (0.69)
	254	1.67 (0.38)	3.74 (0.90)	5.41 (0.59)
	381	1.78 (0.37)	4.86 (0.93)	6.65 (0.75)
40	76	3.00 (0.61)	5.96 (1.12)	8.96 (0.80)
	128	2.75 (0.67)	5.56 (1.13)	8.31 (0.71)
	254	2.74 (0.67)	5.09 (1.60)	7.83 (1.13)
	381	2.94 (0.59)	5.06 (1.08)	8.00 (0.81)
100	76	3.68 (1.01)	7.30 (1.75)	10.99(1.39)
	128	—	—	—
	254	—	—	—
	381	4.50 (0.62)	6.92 (2.3)	11.42 (1.93)

Table III: IMC Layer Thickness from Non-Isothermal Aging, Fast Cycle Rate, Right of center.

Time (Days)	Gap (mm)	Ave. Layer Thickness (Std. Dev.) (μm)		
		Cu_3Sn	Cu_6Sn_5	Total
10	76	1.97 (0.34)	3.23 (0.92)	5.19 (0.65)
	128	1.91 (0.31)	3.19 (1.34)	5.38 (0.44)
	254	1.62 (0.35)	3.67 (1.55)	5.58 (0.70)
	381	1.71 (0.34)	4.46 (0.91)	6.16 (0.60)
40	76	3.00 (0.54)	5.81 (0.97)	8.81 (0.60)
	128	2.72 (0.62)	5.78 (1.02)	8.49 (0.69)
	254	2.81 (0.49)	4.92 (1.02)	7.73 (0.81)
	381	2.78 (0.58)	5.54 (1.00)	8.32(0.64)
100	76	3.63 (0.92)	7.85 (2.03)	11.48 (1.47)
	128	—	—	—
	254	—	—	—
	381	4.57 (0.62)	7.04 (1.69)	11.61 (1.29)

Table IV: IMC Layer Thickness from Non-Isothermal Aging, Slow Cycle Rate.

Time (Days)	Gap (mm)	Ave. Layer Thickness (Std. Dev.) (μm)		
		Cu_3Sn	Cu_6Sn_5	Total
10	76	1.98 (0.32)	4.09 (0.82)	6.07 (0.64)
	128	1.85 (0.50)	4.14 (1.11)	5.99 (0.79)
	254	2.14 (0.37)	4.22 (0.89)	6.36 (0.69)
	381	2.07 (0.39)	4.43 (0.69)	6.49 (0.56)
40	76	3.47 (0.75)	5.83 (1.73)	9.30 (1.19)
	128	3.50 (0.58)	6.11 (1.61)	9.61 (1.13)
	254	4.11 (1.81)	5.24 (2.67)	9.35 (1.60)
	381	3.53 (0.57)	5.74 (1.61)	9.28 (1.24)
100	76	4.47 (1.10)	8.68 (2.58)	13.15 (2.30)
	128	—	—	—
	254	—	—	—
	381	5.50 (1.23)	7.05 (3.00)	12.55 (2.30)

Table V: IMC Layer Thickness from Isothermal Aging at 443 K.

Time (Days)	Gap (mm)	Ave. Layer Thickness (Std. Dev.) (μm)		
		Cu_3Sn	Cu_6Sn_5	Total
10	76	2.67 (0.80)	5.85 (1.43)	8.52 (0.93)
	128	2.79 (0.55)	6.70 (1.28)	9.49 (0.95)
	254	2.62 (0.54)	6.08 (1.37)	8.70 (1.06)
	381	2.63 (0.55)	6.16 (1.20)	8.78 (0.90)
40	76	4.41 (0.94)	11.22 (3.15)	15.64 (2.87)
	128	4.82 (0.91)	9.79 (3.37)	14.61 (2.93)
	254	4.56 (0.90)	10.93 (3.35)	15.49 (2.74)
	381	4.57 (0.84)	10.38 (2.30)	14.95 (1.74)
100	76	7.67 (1.27)	10.97 (3.10)	18.64 (2.29)
	128	7.86 (1.23)	11.44 (2.85)	19.3 (1.94)
	254	6.89 (1.42)	13.33 (3.29)	20.23 (2.60)
	381	7.56 (1.27)	12.78 (3.74)	20.34 (3.14)

Theory

The model for intermetallic layer growth consisted of a set of governing partial and ordinary differential equations and the associated initial and boundary conditions. A summary of those equations is given below, and some pertinent aspects of the numerical implementation of the equations in the computer code are also discussed. Further detail is given in Reference 3.

Governing Equations

A substrate solder system in which I-1 intermetallic layers form and grow between the substrate and bulk solder is shown schematically in Figure 3. Let the substrate form the left boundary of the system, and solder the right boundary. Let $i = 1,2,3,\ldots,I-1$ denote the sequence of intermetallic layers growing from left to right. That is, $i = 1$ denotes the layer adjacent to the right edge of the substrate ($i = 0$), and $i = I-1$ denotes the layer adjacent to the left edge of the solder ($i = I$). Growth of the intermetallic layers results from interfacial reaction and diffusion of a binary set of interacting constituents. In each layer, the diffusion of either constituent can be rate controlling.

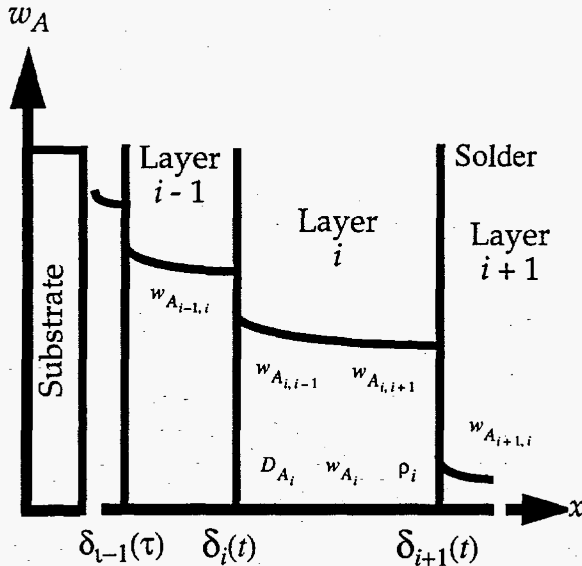

Figure 3. Schematic diagram of intermetallic layer growth between substrate and solder.

Let T denote temperature; t denote time; x denote position with respect to a fixed origin; $\delta_i(t)$ the position of the interface between layer i-1 and layer i, and $\Delta_i(t)$ the thickness of layer i

$$\Delta_i(t) = \delta_{i+1}(t) - \delta_i(t) \tag{1}$$

Then, for $\delta_i(t) < x < \delta_{i+1}(t)$, the material balance for the rate controlling constituent in each layer is given by

$$\frac{\partial w_{A_i}}{\partial t} = \frac{\partial}{\partial x}\left(D_{A_i}\frac{\partial w_{A_i}}{\partial x}\right) \tag{2}$$

where w_{A_i} denotes the mass fraction of the rate-controlling constituent in layer i, and D_{A_i} denotes the diffusion coefficient, which is an effective diffusion coefficient analogous to the chemical diffusion coefficient discussed by Shewmon (5), and which can be a function of x, t, w_{A_i}, and T, and specified accordingly. For frequent cases of interest, the diffusion coefficient D_{A_i} is given by an Arrhenius expression

$$D_{A_i} = D_{A_{i_0}}[\exp Q_{A_i}/(RT)] \tag{3}$$

where $D_{A_{i_0}}$ is a constant; Q_{A_i} is the activation energy for diffusion of the constituent in layer i, and R is the gas constant. In general, the temperature T can be a function of x and t, which also can be specified.

When constituent diffusion and interface displacement are not hindered by finite material boundaries, and the rate R_i of interfacial chemical reaction is sufficiently fast, local chemical equilibrium exists at the interface, and the concentrations of the diffusing constituents in layer i are essentially constant at $\delta_i(t)$. Therefore, at $\delta_i(t)$, the boundary condition for Eq. 2 is

$$(w_{A_i})_{\delta_i^r} = \text{constant} = (w_{A_i}{}^*)_{\delta_i^r} \tag{4}$$

and if local equilibrium exists at $\delta_{i+1}(t)$, the boundary condition is

$$(w_{A_i})_{\delta_{i+1}^l} = \text{constant} = (w_{A_i}{}^*)_{\delta_{i+1}^l} \tag{5}$$

where $(w_{A_i}{}^*)_{\delta_i^r} \neq (w_{A_i}{}^*)_{\delta_{i+1}^l}$, and superscripts l and r denote values at the left and right sides of the interface, respectively. The initial condition for Eq. 2 is

$$w_{A_i}(x, 0) = f_i(x) \tag{6}$$

where $f_i(x)$ is known or assumed.

When the rate R_i of interfacial reaction is slow enough to preclude local equilibrium at the interface, the constant concentration boundary conditions given by Eqs. 4 and 5 must be replaced by flux-type boundary conditions given by

$$-\rho_i D_{A_i}\left(\frac{\partial w_{A_i}}{\partial x}\right)_{\delta_i^r} = R_i^r \tag{7}$$

$$\rho_i D_{A_i}\left(\frac{\partial w_{A_i}}{\partial x}\right)_{\delta_{i+1}^l} = R_{i+1}^l \tag{8}$$

Furthermore, when constituent diffusion encounters a finite material boundary, the boundary condition for Eq. 2 becomes the zero flux condition at that boundary.

The displacement of each interface is given by

$$\left[\rho_{i-1}(w_{A_{i-1}})_{\delta_i^l} - \rho_i(w_{A_i})_{\delta_i^r}\right]\frac{d\delta_i}{dt} = -\rho_{i-1}D_{A_{i-1}}\left(\frac{\partial w_{A_{i-1}}}{\partial x}\right)_{\delta_i^l} + \rho_i D_{A_i}\left(\frac{\partial w_{A_i}}{\partial x}\right)_{\delta_i^r} \tag{9}$$

where ρ_i denotes the mass density of layer i. The initial condition for Eq. 9 is

$$\delta_i(t = 0) = \delta_i^0 = \text{a constant} \tag{10}$$

For purposes of analysis, the interfacial reaction rates can be expressed by generic linear-driving-force expressions of the form

$$R_i^r = k_i^r \rho_i \left[(w_{A_i}^*)_{\delta_i^r} - (w_{A_i})_{\delta_i^r} \right] \tag{11}$$

and

$$R_{i+1}^l = k_{i+1}^l \rho_i \left[(w_{A_i})_{\delta_{i+1}^l} - (w_{A_i}^*)_{\delta_{i+1}^l} \right] \tag{12}$$

which are useful for examining order of magnitude effects. The rate constants such as k_i^r can be represented by Arrhenius expressions, such as

$$k_i^r = k_{i_0}^r \exp(E_i^r/(RT)) \tag{13}$$

where $k_{i_0}^r$ is a constant and E_i^r is the activation energy for interfacial reaction.

Numerical Implementation

In this work the numerical approach adopted to solve the system of coupled diffusion and interface displacement equations given by Eqs. 2 and 9 for each layer was the method of lines (6), which uncouples the spatial and temporal discretization of the partial differential equations. In this application the spatial discretization is represented by finite differences which results in a set of coupled, first-order, ordinary differential equations (ODE) in time. These are solved in turn by an efficient library ODE solver that determines the time stepping internally to maintain stability. The implicit solution procedure of the ODE solver uses a variable order (one through five) backward difference formulation (7, 8). The implementation of the method of lines for solving reactive diffusion equations adopted in this work was that of Baer, et al (9). This implementation includes an adaptive meshing scheme that automatically resolves steep mass fraction gradients and will return to a coarser grid as the gradient relaxes. A transformation of the spatial coordinate x given by

$$\bar{x}_i = \frac{x - \delta_i(t)}{\Delta_i(t)} \tag{14}$$

was used to circumvent the need to remesh the growing or shrinking layers. In which case, for
$\delta_i < x < \delta_{i+1}$, or $0 < \bar{x}_i < 1$, Eq. 2 becomes

$$\frac{\partial w_{A_i}}{\partial t} = \frac{1}{\Delta_i^2} \frac{\partial}{\partial x}\left(D_{A_i} \frac{\partial w_{A_i}}{\partial \bar{x}} \right) + F(\bar{x}_i, \delta_i, \Delta_i) \frac{\partial w_{A_i}}{\partial \bar{x}} \tag{15}$$

where

$$F(\bar{x}_i, \delta_i, \Delta_i) = \left(\frac{1}{\Delta_i} \frac{d\delta_i}{dt} + \frac{\bar{x}_i}{\Delta_i} \frac{d\Delta_i}{dt} \right) \tag{16}$$

At $x = \delta_i(t)$, or $\bar{x}_i = 0$, Eq. 9 becomes

$$\left[\rho_{i-1} (w_{A_{i-1}})_{\bar{x}_{i-1} = 1} - \rho_i (w_{A_i})_{\bar{x}_i = 0} \right] \frac{d\delta_i}{dt} = -\frac{\rho_{i-1} D_{A_{i-1}}}{\Delta_{i-1}} \left(\frac{\partial w_{A_{i-1}}}{\partial \bar{x}_{i-1}} \right)_{\bar{x}_{1-1} = 1} + \frac{\rho_i D_{A_i}}{\Delta_i} \left(\frac{\partial w_{A_i}}{\partial \bar{x}_i} \right)_{\bar{x}_i = 0} \tag{17}$$

and at $x = \delta_{i+1}(t)$, or $\bar{x}_i = 1$,

$$\left[\rho_i (w_{A_i})_{\bar{x}_i = 1} - \rho_{i+1} (w_{A_{i+1}})_{\bar{x}_{i+1} = 0} \right] \frac{d\delta_i}{dt} = -\frac{\rho_i D_{A_i}}{\Delta_i} \left(\frac{\partial w_{A_i}}{\partial \bar{x}_i} \right)_{\bar{x}_i = 1} + \frac{\rho_{i+1} D_{A_{i+1}}}{\Delta_{i+1}} \left(\frac{\partial w_{A_{i+1}}}{\partial \bar{x}_{i+1}} \right)_{\bar{x}_{i+1} = 0} \tag{18}$$

Modeling

Comparison of Numerical and Analytical Results

In previous work (3), results from the one-dimensional code were verified by comparing the numerical results with analytical solutions for simple isothermal systems involving two, three, and five layers. In the present work, the updated version of the code was further verified by comparing numerical results with the analytical solution for a simple two-layer, two-constituent system involving a "reasonable" temperature history and representative Arrhenius parameters. The comparison showed good agreement between numerical and analytical results and is described below.

To compare numerical and analytical results, the hypothetical case illustrated schematically in Figure 4 was used and consisted of a substrate and solder material with which the substrate could form a solid solution. At time $t = 0$, the substrate and solder are uniformly contacted along a planar interface at $x = 0$. The substrate occupies the space at $x < 0$, and the solder at $x > 0$. At $t > 0$, the substrate dissolves in the solder and the interface position $\delta_1(t)$ between the substrate and solder phase displaces in the direction of $x < 0$. The solubility of the substrate in the solder is denoted by S_{A_1}, and the solubility of the solder material in the substrate is negligible. Volume changes due to dissolution of the substrate are also negligible, and the densities of the substrate and solder phase are equal. The variation of the temperature T with respect to time t is slow enough so that T is spatially uniform, and values of t are small enough so that both substrate and solder can be considered semi-infinite. The intrinsic rate R_1^r of interfacial reaction between solder and substrate is relatively fast so that local chemical equilibrium exists at the substrate-solder interface, and the rate of dissolution is controlled by diffusion of the substrate material, denoted by subscript A into the solder phase. Diffusion of the substrate material into the solder is adequately described by Fick's law with an Arrhenius-type diffusion coefficient.

The mass balance for the substrate material diffusing into the

solder is given by

$$\frac{\partial w_{A_1}}{\partial t} = \frac{\partial}{\partial x}\left(D_{A_1}\frac{\partial w_{A_1}}{\partial x}\right) \quad (19)$$

where w_{A_1} denotes the mass fraction of the substrate material in the solder, and D_{A_1} denotes the diffusion coefficient, which is given by an Arrhenius expression

$$D_{A_1} = D_{A_{1_0}}\exp[Q_{A_1}/(RT)] \quad (20)$$

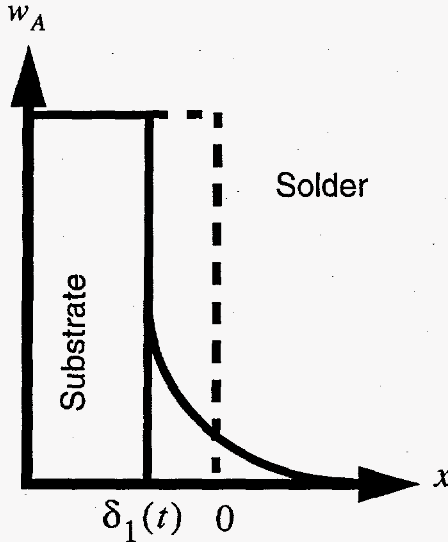

Figure 4. Schematic diagram of substrate-solder system. Initially, the interface between the substrate and solder is at $x = 0$, as indicated by the dashed line.

where $D_{A_{1_0}}$ is a constant; Q_{A_1} is the activation energy for diffusion of the substrate material in the solder, and R is the gas constant. The temperature T is a known function of the time t as discussed below. The boundary conditions for Eq. 19 are

$$(w_{A_1})_{\delta_1^r} = \text{constant} = S_{A_1} \quad (21)$$

and

$$w_{A_1}(x \to \infty) = 0 \quad (22)$$

and the initial condition is

$$w_{A_1}(x > 0) = 0 \quad (23)$$

The displacement of the interface at $\delta_1(t)$ is described by

$$\left[\rho_0(w_{A_0} = 1)_{\delta_1^l} - \rho_1(w_{A_1})_{\delta_1^r}\right]\frac{d\delta_1}{dt} = \rho_1 D_{A_1}\left(\frac{\partial w_{A_1}}{\partial x}\right)_{\delta_1^r} \quad (24)$$

where ρ_0 and ρ_1 denotes the mass density of substrate and solder, respectively; δ_1^l and δ_1^r denote the value of $\delta_1(t)$ approached from lesser and greater values of x, respectively, and

$$\delta_1(t = 0) = 0 \quad (25)$$

Letting

$$\tau(t) = \int_0^t D_{A_1}[T(t')]dt' \quad (26)$$

Eqs. 19 - 25 can be solved analytically to obtain the following expressions for $w_{A_1}[x, \tau(t)]$ and $\delta_1[\tau(t)]$

$$w_{A_1}[x, \tau(t)] = S_{A_1}\left[\frac{\text{erfc}(\eta)}{\text{erfc}(\gamma)}\right] \quad (27)$$

and

$$\delta_1[\tau(t)] = 2\gamma\sqrt{\tau(t)} \quad (28)$$

where

$$\eta = \frac{x}{2\sqrt{\tau(t)}} \quad (29)$$

and

$$\gamma = \left(\frac{1}{\sqrt{\pi}}\right)\left(\frac{S_{A_1}}{1 - S_{A_1}}\right)\left[\frac{\exp(-\gamma^2)}{\text{erfc}(\gamma)}\right] = \text{constant} \quad (30)$$

Results from the one-dimensional code were compared with this analytical solution for two cases. In both cases, the temperature varied sinusoidally over a period of one day with a minimum temperature of 298 K to a maximum of 498 K. The solubility of the substrate in the solder, S_{A_1}, was 0.05. Also, as previously stated, the solubility of the solder material in the substrate was negligible; volume changes due to dissolution of the substrate were negligible, and the densities of the substrate and solder phase were equal and constant. The analytical solution assumes zero initial thickness for the intermetallic layers (Eq. 23), while the numerical solution requires an initial thickness to be specified, in many cases, the process being modeled begins with a small but finite thickness of these layers. In cases where a layer appears to be initially absent, the initial thickness specified in the code can be made small enough to adequately approximate the system being modeled. The diffusion coefficient was given by Eq. 3. For Case 1, DA_{1_0} was 1.8 x 10^{-4} m^2/s, and the activation energy Q_{A_1} was 126 kJ/mole. For Case 2, DA_{1_0} was 3.1 x 10^9 m^2/s, and Q_{A_1} was 252 kJ/mole. These values were selected to provide a large range of typical values. For Case 1, the resulting diffusion coefficient, D_{A_1}, varied from a value of 1.5 x 10^{-26} m^2/s at 298 K to a value of 1.2 x 10^{-17}at 498 K. For Case 2, the diffusion coefficient D_{A_1} varied from a value

of 2.2 x 10^{-35} to 1.2 x 10^{-17} over the same temperature range. Calculations were carried out to a time of 225 days (*i.e.*, 225 cycles). The agreement between the numerical and analytical solutions was excellent and is illustrated for Case 1 in Figures 5 - 7. Figures 5 and 6 show the interface location, $\delta_1(t)$, as a function of time; Eq. 25 defines the initial position of the interface. Figure 7 shows the spatial distribution of mass fraction, w_{A_1}, at three selected times.

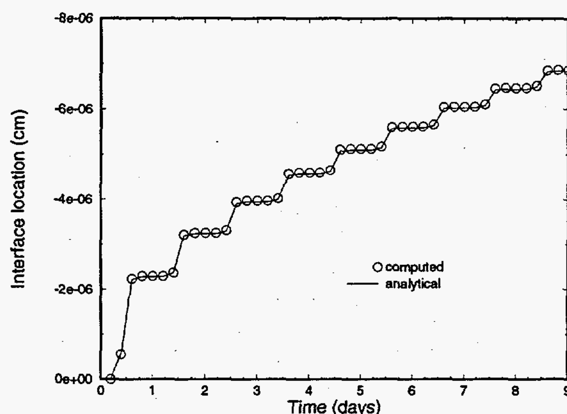

Figure 5. Time history of interface location for Case 1, t=0 to 9 days.

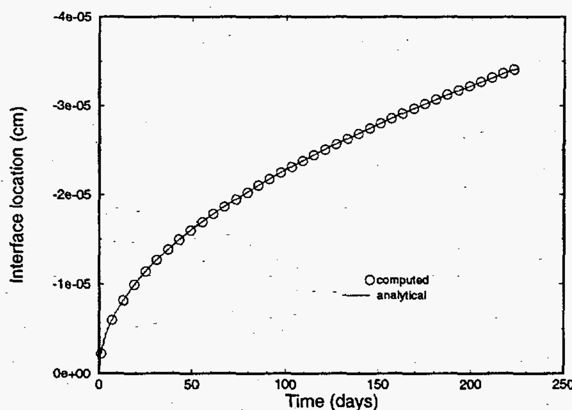

Figure 6. Time history of interface location for Case 1, t=0 to 225 days.

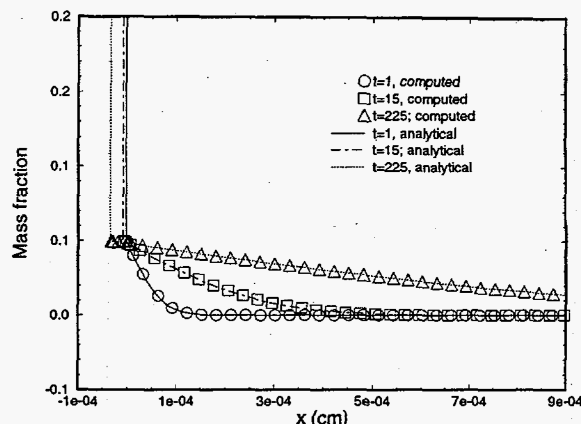

Figure 7. Profile of mass fraction (<0.2) for Case 1, t=1, 15 and 225 days.

Application to Experimental Data

For each temperature history intermetallic layer growth was predicted using a four-layer model that consisted of Cu, Cu_3Sn, Cu_6Sn_5, and Sn layers, denoted by subscripts 1, 2, 3, and 4, respectively. The Pb-rich Pb-Sn layer was neglected because Cu was not detected in the layer. Also, since the experimental data indicated that diffusion of Sn into the Cu substrate and diffusion of Cu into the bulk Pb-Sn phases were negligible, two diffusion equations (Eq. 2) were required, one each for the Cu_3Sn and Cu_6Sn_5 layers, and three interface displacement equations, one each for the interface $d_1(t)$ between Cu and Cu_3Sn, $d_2(t)$ between Cu_3Sn and Cu_6Sn_5, and $d_3(t)$ between Cu_6Sn_5 and Sn. However, the available experimental data does not permit the evaluation of separate diffusion coefficients for Cu and Sn, and since the choice of constituent does not alter the overall effect of bulk diffusion, for convenience, the numerical predictions were based on diffusion of Cu. Local equilibrium was assumed at each side of $d_1(t)$, $d_2(t)$, and $d_3(t)$. The constant concentration boundary conditions given by Eqs. 4 and 5 were then evaluated from the Cu-Sn phase diagram and are shown in Table VI, which also includes the mass density of each layer.

Table VI: Interfacial mass fractions and mass densities for four-layer model.

Layer	$(w_{A_i})_{\delta_i^r}$	$(w_{A_i})_{\delta_{i+1}^l}$	$\rho_i \times 10^{-3}$ (kg/m^3)
Cu (1)	1.000	1.000	8.9
Cu_3Sn (2)	0.623	0.605	9.0
Cu_6Sn_5 (3)	0.410	0.400	8.4
Sn (4)	0.000	0.000	7.3

Arrhenius expressions for the effective diffusion coefficients D_{A_i} based on diffusion of Cu were evaluated previously (3).

Values for the parameters in Eq. 3 for Cu_3Sn and Cu_6Sn_5 layers are given in Table VII.

Table VII: Arrhenius parameters in Eq. 3 for Cu_3Sn and Cu_6Sn_5.

Intermetallic Layer	$D_o \times 10^8$ (m^2/s)	Q (kJ/mol)
Cu_3Sn	1.18	71.7
Cu_6Sn_5	43.4	80.3

As mentioned previously, the earlier isothermal studies (3) indicated that Cu_3Sn and Cu_6Sn_5 layer growth are generally consistent with a bulk diffusion mechanism, but the diffusion coefficient is probably not constant. During early layer growth, diffusion appears to be faster than during later growth. Similar effects have been reported previously by Kofstad (10), who used the term "enhanced diffusion" to indicate effects which could be attributed to grain boundary diffusion, residual strain, and poor crystallization during early layer growth.

To empirically account for the effects of enhanced diffusion during early layer growth, a variable diffusion coefficient $\overline{D_{A_i}}$ defined by

$$\overline{D_{A_i}} = D_{A_i} + D'_{A_i} \exp(-\lambda_i \Delta_i) \quad (31)$$

was used (3). On the right side of Eq. 31, the term involving D'_{A_i} represents the contribution from the enhanced diffusion process that occurs during early layer growth and then becomes negligible as the layer thickness increases, so that for thick layers, $\overline{D_{A_i}}$ reduces to the "equilibrium" value D_{A_i} given by Eq. 3. Reasonable analytical expressions for the temperature dependence of D'_{A_i} and λ_i have not yet been obtained. Since layer growth resulting from nonisothermal temperature histories was dominated by the periods of time at 443 K, the values of D'_{A_i} and λ_i obtained previously (3) at 443 K were used to predict layer growth for all three temperature histories and are given in Table VIII.

Table VIII: Values of D'_A and λ (Eq. 31) Cu_3Sn and Cu_6Sn_5 at 443 K.

Intermetallic Layer	$D'_A \times 10^{16}$ (m^2/s)	$\lambda \times 10$ (m^{-1})
Cu_3Sn	9.3	20.0
Cu_6Sn_5	4.2	3.8

Finally, since the initial thicknesses of the Cu_3Sn and Cu_6Sn_5 layers in the samples used in the thermal aging experiments were not available, layer growth was predicted by starting with the layer thickness determined experimentally at 10 days and then predicting layer growth during the next 90 days. The resulting predicted layer growth as a function of time for both the Cu_3Sn and Cu_6Sn_5 layers are shown in Figures 8 - 10, for the *isothermal*, *nonisothermal*, *slow-cycle*, and *nonisothermal*, *fast cycle*, respectively.

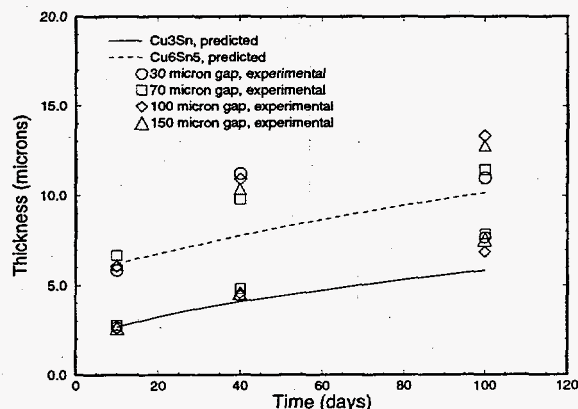

Figure 8. Experimental and numerical results for *isothermal* aging experiments at 443 K. Experimental data are from Table V.

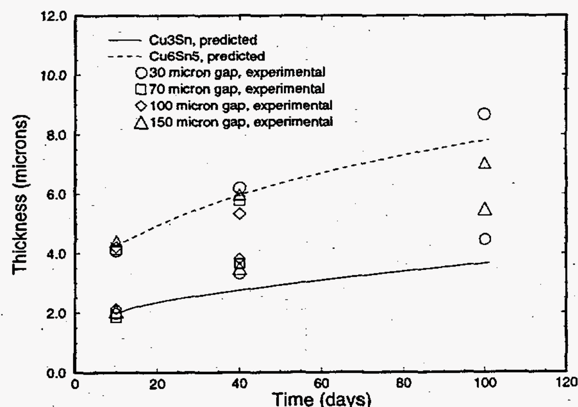

Figure 9. Experimental and numerical results for *nonisothermal, slow-cycle* aging experiments. Experimental data are from Table IV.

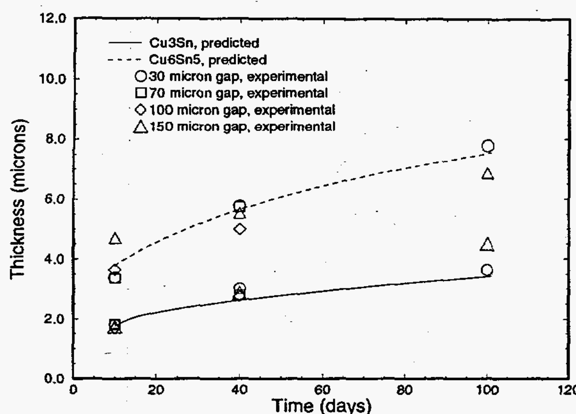

Figure 10. Experimental and numerical results for *noniso-thermal, fast-cycle* aging experiments. Experimental data are combined values for data in Tables I - III.

Discussion

The agreement between the predicted and experimental results shown in Figures 8-10 is generally good, particularly since the predictions were made using parameter values obtained in the previous experimental work (3). No parameter fitting or adjustments were made using data from the current isothermal or nonisothermal experiments. While in some cases, predicted layer growth was less than experimentally observed, the differences were small and on the order of the experimental error. Furthermore, minor differences between the sample materials and preparation procedures used in the current experiments and those used in the previous isothermal studies could cause small variations in the initial microstructure of the joint materials which would affect enhanced diffusion during early layer growth. For example, sample geometry, quench rate, dissolved oxygen and solder composition, and solder bath temperature all probably have some influence on the initial IMC layer properties, particularly with respect to enhanced diffusion during early layer growth in the aging experiments.

The most prominent differences between predicted and experimentally observed layer growth appeared to occur with the isothermal experiments at 443 K. Therefore, it appears reasonable to assume that temperature cycling was not responsible for the differences between predicted and experimental results, and that nonisothermal IMC layer growth can be modeled using temperature-dependent parameter values obtained from independent isothermal experiments. More detailed models for layer growth, particularly with respect to enhanced diffusion during early growth and microstructural changes during thermal aging, would probably reduce the differences between predicted and experimentally observed results.

Conclusions

Nonisothermal IMC layer growth in the 63Sn-37Pb/Cu system was reasonably predicted using the model/code described above and temperature-dependent parameter values obtained from independent isothermal experiments. More detailed models for layer growth, particularly with respect to microstructural evolution during joint formation and subsequent layer growth during thermal aging would further improve predictive capabilities, especially regarding the effects of enhanced diffusion during early layer growth.

Acknowledgments

The authors gratefully acknowledge the technical assistance provided by A. Carter, IMC layer thickness measurements, and J. Rejent, experimental work, both of Sandia National Laboratories.

References

1. P. T. Vianco, K. L. Erickson, and P. L. Hopkins, "Solid State Intermetallic Compound Growth Between Copper and High Temperature Tin-Rich Solders - Part I: Experiment," Journal of Electronic Materials, 23 (1994) 721.

2. K. L. Erickson, P. L. Hopkins, and P. T. Vianco, "Solid State Intermetallic Compound Growth Between Copper and High Temperature Tin-Rich Solders - Part II: Modeling," Journal of Electronic Materials, 23 (1994) 729.

3. K. L. Erickson, P. L. Hopkins, and P. T. Vianco, "Analysis of Physiochemical Processes During Solder Aging" (Report SAND94-0691, Sandia National Laboratories, 1994).

4. ASM Handbook, vol. 6 (Metals Park, OH: ASM Intern., 1993) 992.

5. Paul Shewmon, Diffusion in Solids, second edition (Warrendale, Pennsylvania: The Minerals, Metals & Materials Society, 1989) 131-135.

6. J. M Hyman, "Method of Lines Approach to the Numerical Solution of Conservation Laws" (Report LA-UR-79-837, Los Alamos Scientific Laboratory, 1979).

7. L. F. Shampine, and H. A. Watts, "DEPAC-Design of a User Oriented Package of ODE Solvers" (Report SAND79-2374, Sandia National Laboratories, 1980).

8. A. C. Hindmarsh, "ODE Solvers for Use with the Method-of-Lines" (Report UCRL-85293 (Rev. 1), Lawrence Livermore National Laboratory 1981).

9. M. R. Baer, et al., "Modeling and Computation of Deflagration-to-Detonation Transition (DDT) in Reactive Granular Materials", Lectures in Applied Mechanics, 24 (1986).

10. P. Kofstad, High Temperature Oxidation of Metals (New York, NY: John Wiley & Sons, Inc. 1966) 140 -144.